Supplemental Online Materials

Shock and Post-Shock Temperatures in an Ice-Quartz Mixture: Implications for Melting During Planetary Impact Events

R. G. Kraus[1], S. T. Stewart[1], A. Seifter[2], A. W. Obst[2]

[1]Department of Earth and Planetary Sciences,
Harvard University, Cambridge, Massachusetts, USA
[2]Los Alamos National Laboratory, Physics Division,
Los Alamos, New Mexico, USA

The supplemental material for this article contains:

1. Table S1 provides shock wave equation of state parameters used in impedence match solution to determine peak pressure in shocked mixture.
2. Figure S1 showing visible and near-infrared radiance data and fits from 7.9 GPa experiment.
3. Figure S2 showing visible and near-infrared radiance data and fits from 12.9 GPa experiment.
4. Figure S3 showing visible and near-infrared radiance data and fits from 16.2 GPa experiment.
5. Figure S4 showing post-shock radiance data and fits from 18.5 GPa experiment.
6. Figure S5 showing solution to one-dimensional thermal diffusion equation for H_2O-SiO_2 interface.
7. Figure S6 showing idealized one-dimensional diagram of radiating mixture used to derive the emissivity and area fraction of H_2O
8. Text S1 derives the one-dimensional radiation absorption analysis used in multi-component hotspot fit.
9. Text S2 provides experimental details.

Table S1: Hugoniot equation of state ($U_s = C_0 + su_p$) used in impedence match solution for peak shock pressure in mixture. The release isentrope of the driver is assumed to be the reflected Hugoniot.

Material	ρ_0 [g/cm^3]	C_0 [km/s]	s	Reference
304 Stainless Steel (flyer)	7.896	4.569	1.49	Steinberg (1991)
Al-2024 (driver)	2.785	5.23	1.32	Steinberg (1991)

Figure S1: Thermal radiation emitted from a mixture of H_2O and SiO_2 subjected to a 7.9 GPa planar shock wave. For 0.65, 0.81, 1.8, and 2.3 μm, black lines are fits using equation 2. For 3.5 and 4.8 μm, black lines denote time interval used to determine post-shock temperatures.

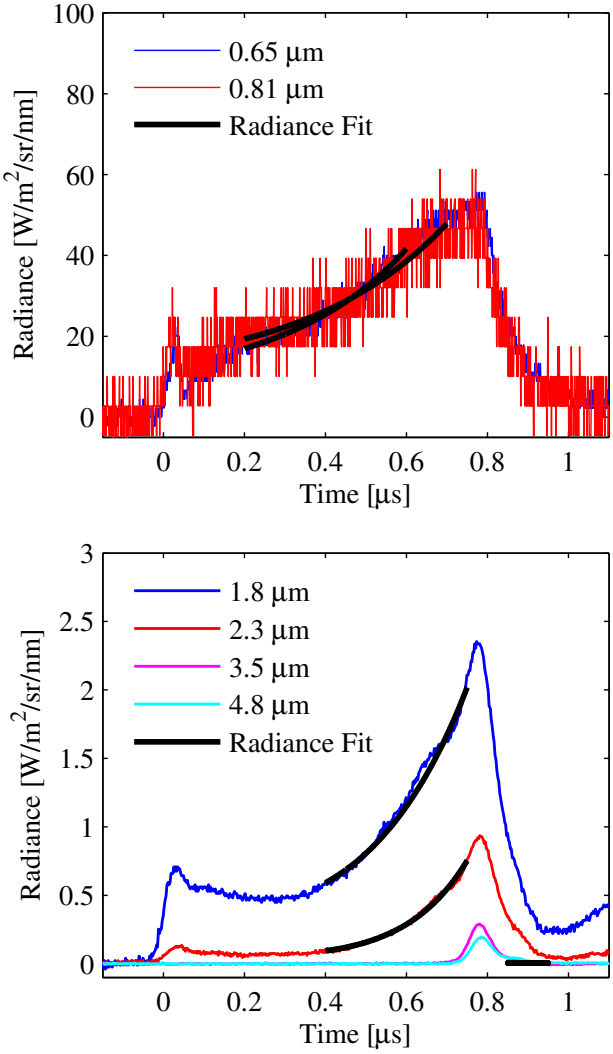

Figure S2: Thermal radiation emitted from a mixture of H_2O and SiO_2 subjected to a 12.9 GPa planar shock wave. For 0.65, 0.81, 1.8, and 2.3 μm, black lines are fits using equation 2. For 3.5 and 4.8 μm, black lines denote time interval used to determine post-shock temperatures.

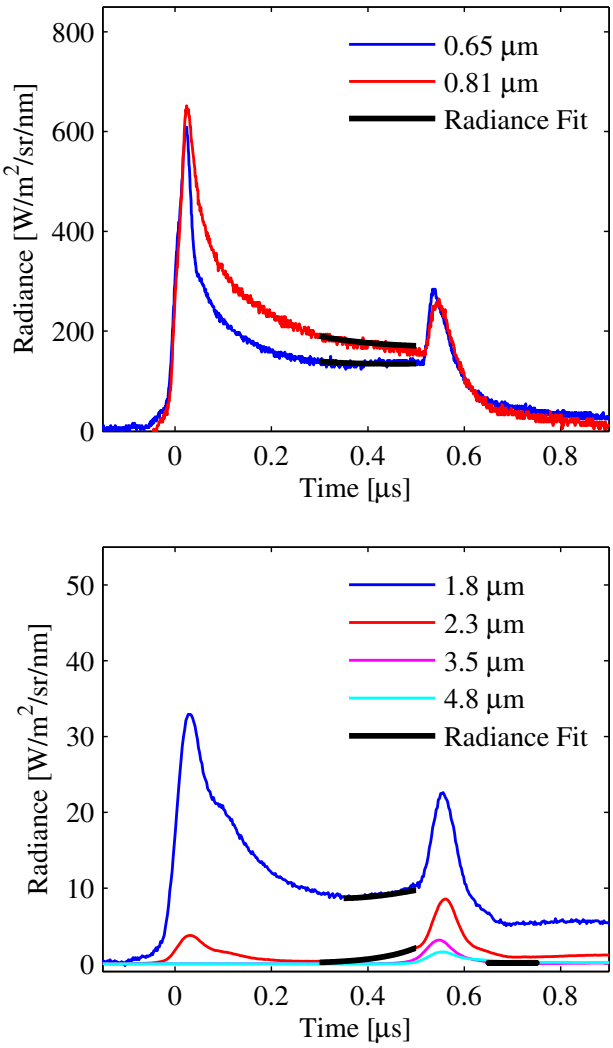

Figure S3: Thermal radiation emitted from a mixture of H_2O and SiO_2 subjected to a 16.2 GPa planar shock wave. For 0.65, 0.81, 1.8, and 2.3 μm, black lines are fits using equation 2. For 3.5 and 4.8 μm, black lines denote time interval used to determine post-shock temperatures.

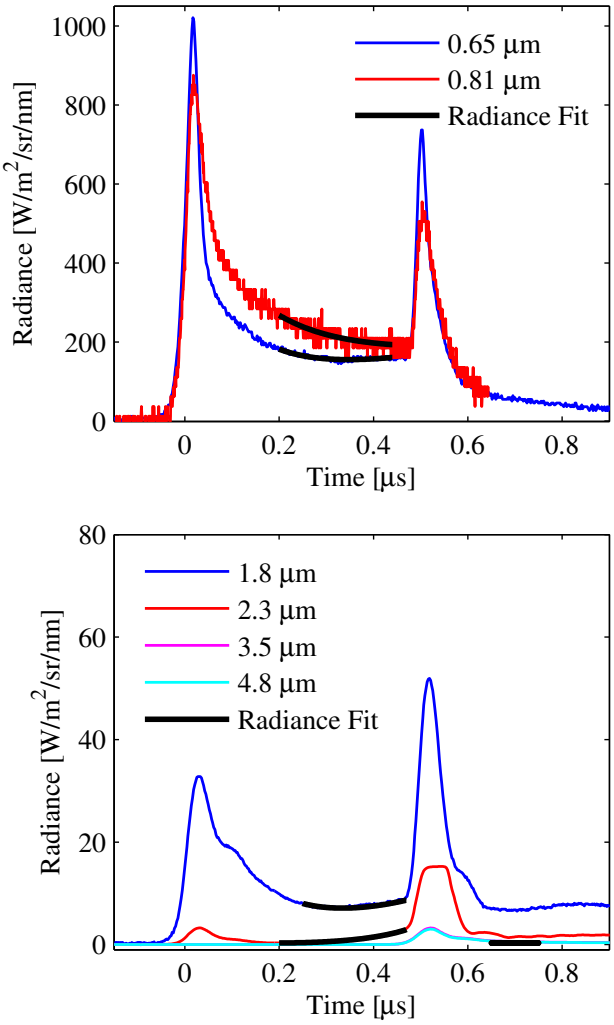

Figure S4: Post-shock thermal radiation emitted from a 40:60 volumetric mixture of H_2O and SiO_2 subjected to a 18.5 GPa planar shock wave. For 3.5 and 4.8 μm, black lines denote time interval used to determine post-shock temperatures. Detectors were saturated at shorter wavelength channels and consequently a shock temperature could not be obtained.

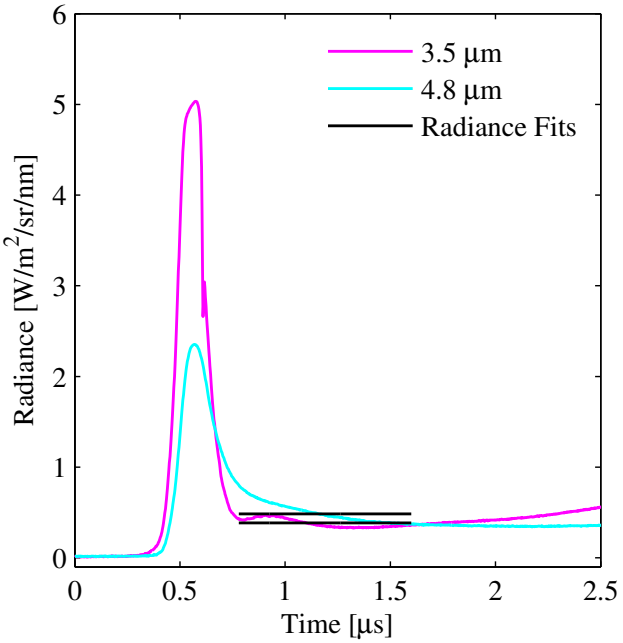

Figure S5: Numerical solution to the thermal diffusion equation across an interface between H_2O and SiO_2, accounting for their different thermal transport properties. Initial conditions were 22.7 GPa and the shock temperature on the principal Hugoniot of each component. The shock temperature in the H_2O was determined from the 5-phase equation of state model for H_2O (Senft and Stewart, 2008), and the shock temperature in the SiO_2 was taken from calculations by Wackerle (1962). The temperature at the interface was solved exactly using the method described in Carslaw and Jaeger (1946), and the temperatures within the H_2O and SiO_2 were determined by integrating the thermal diffusion equation by a first-order accurate finite difference technique. Note that the conclusion that thermal diffusion is negligible during the experiment is robust to a wide variations in material parameters.

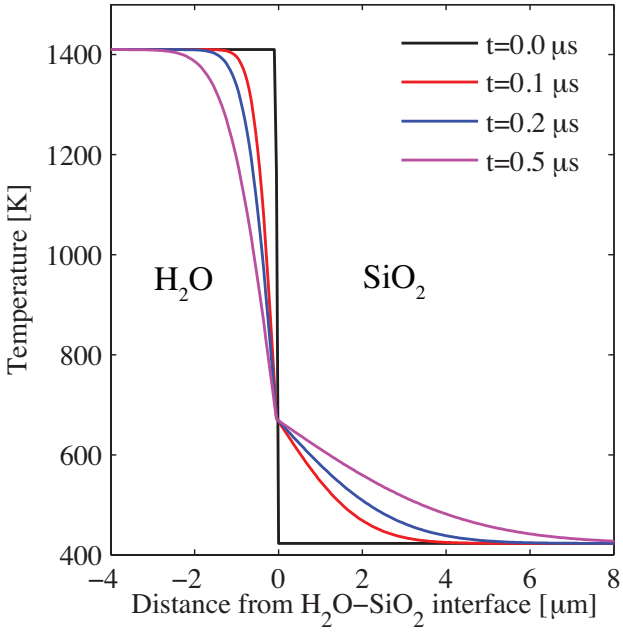

Figure S6: Schematic of one-dimensional radiation absorption (black arrows pointing to the left) and radiance emitted (red arrows pointing to the right) in a mixture of H_2O and SiO_2. The radiance from the free surface, L_ϵ, is the sum of the radiation emitted from each cell of H_2O and SiO_2, $\epsilon_H L_H$ and $\epsilon_S L_S$, minus the radiation absorbed by each cell of H_2O and SiO_2, $L_{abs}(a_H, d_H)$ and $L_{abs}(a_S, d_S)$ respectively. Here a_H and a_S are the wavelength dependent optical absorption coefficients in H_2O and SiO_2, respectively, and d_H and d_S are the average thicknesses of the cells of H_2O and SiO_2, respectively.

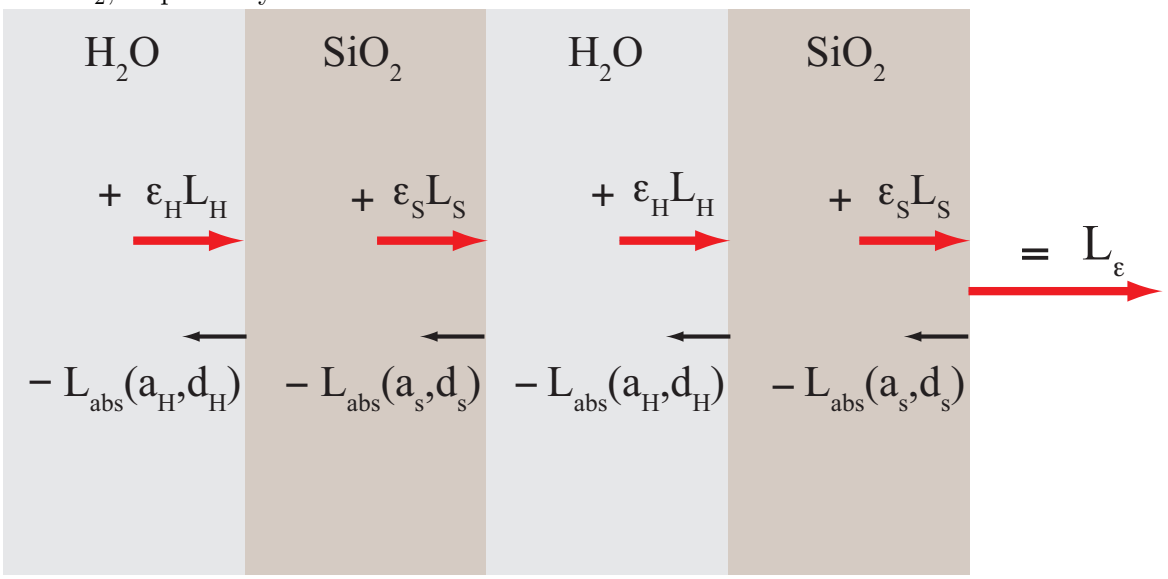

Text S1:
From Kirchoff's law we know that the emissivity is related to the coefficient of absorption 'a' by Equation (S1), where d is the thickness of the radiating material.

$$\epsilon = 1 - e^{-ad} \tag{S1}$$

Now consider the one-dimensional geometry of alternating plates of H_2O and SiO_2, as shown in Figure S6; the H_2O and SiO_2 have absorption coefficients of a_H and a_S, respectively. Heat the plates so they begin emitting thermal radiation. The emitted radiation from the free surface of the mixture will be the superposition of light emitted from the individual layers, $\epsilon_H L_H$ and $\epsilon_S L_S$ respectively, minus the light absorbed by the layers in the path of the radiation. Neglecting internal reflections, the radiance emitted from such a surface, L_ϵ, is described by Equation (S2), where $\epsilon_i = \left(1 - e^{-a_i d_i}\right)$, and d_i is the thickness of plate type 'i'.

$$L_\epsilon = L_S\epsilon_S + L_H\epsilon_H e^{-a_S d_S} + L_S\epsilon_S e^{-a_H d_H} e^{-a_S d_S} + L_H\epsilon_H e^{-2a_S d_S} e^{-a_H d_H} + L_S\epsilon_S e^{-2a_H d_H} e^{-2a_S d_S} + ... \tag{S2}$$

Assuming there are '$2N$' plates, one can separate the sum over the radiation emitted from the separate types of plates, shown in Equation (S3).

$$L_\epsilon = L_S\epsilon_S \sum_{n=0}^{N-1} e^{-na_H d_H} e^{-na_S d_S} + L_H\epsilon_H e^{-a_S d_S} \sum_{n=0}^{N-1} e^{-na_H d_H} e^{-na_S d_S} \tag{S3}$$

However, this sum is simply a finite geometric series of the form $\sum_0^{N-1} Ra^n$, which can be simplified to the form shown in Equation (S4).

$$L_\epsilon \approx L_S\epsilon_S \frac{\left(1 - e^{-Na_H d_H} e^{-Na_S d_S}\right)}{\left(1 - e^{-a_H d_H} e^{-a_S d_S}\right)} + L_H\epsilon_H e^{-a_S d_S} \frac{\left(1 - e^{-Na_H d_H} e^{-Na_S d_S}\right)}{\left(1 - e^{-a_H d_H} e^{-a_S d_S}\right)} \tag{S4}$$

This expression is not sufficient to describe emission from a mixture that is heterogeneous in three dimensions as there is an asymmetric term related to whichever plate is at the free surface, this term being $e^{-a_s d_s}$ in Equation (S4) derived for the geometry shown in Figure S6. To fully describe emission from an isothermal mixture of H_2O and SiO_2 one could envision the case where columns of alternating plates are stacked adjacent to each other in such a way that the physical area fractions of H_2O and SiO_2 at the free surface, α_H^P and α_S^P, match what would be measured experimentally if the real samples of H_2O and SiO_2 were sectioned and analyzed to determine relative area fractions. As we can measure the relative volume fractions of H_2O and SiO_2, V_H and V_S, for the samples used in the experiments, we can determine their relative area fractions using Equation (S5) and the fact that the area fractions must add up to one.

$$\frac{\alpha_H^P}{\alpha_S^P} = \left(\frac{V_H}{V_S}\right)^{\frac{2}{3}} \tag{S5}$$

By combining Equations (S4) and (S5), we can fully describe emission from a heterogeneous isother-

mal mixture of H_2O and SiO_2, shown in the follow equation.

$$\begin{aligned} L_\epsilon &= \alpha_S^P \left[L_S \epsilon_S \frac{\left(1 - e^{-Na_H d_H} e^{-Na_S d_S}\right)}{\left(1 - e^{-a_H d_H} e^{-a_S d_S}\right)} + L_H \epsilon_H e^{-a_S d_S} \frac{\left(1 - e^{-Na_H d_H} e^{-Na_S d_S}\right)}{\left(1 - e^{-a_H d_H} e^{-a_S d_S}\right)} \right] \\ &\quad + \alpha_H^P \left[L_S \epsilon_S e^{-a_H d_H} \frac{\left(1 - e^{-Na_H d_H} e^{-Na_S d_S}\right)}{\left(1 - e^{-a_H d_H} e^{-a_S d_S}\right)} + L_H \epsilon_H \frac{\left(1 - e^{-Na_H d_H} e^{-Na_S d_S}\right)}{\left(1 - e^{-a_H d_H} e^{-a_S d_S}\right)} \right] \end{aligned}$$

With regards to a shock wave experiment, we have discussed in the paper how the radiation emitted from the SiO_2 grains is insignificant with respect to the radiation emitted from the H_2O because of the much lower temperature in the SiO_2. This reasonable assumption of neglecting the radiation emitted from the SiO_2 significantly reduces the complexity of L_ϵ.

$$L_\epsilon = \left(\alpha_H^P + \alpha_S^P e^{-a_S d_S}\right) L_H \epsilon_H \frac{\left(1 - e^{-Na_H d_H} e^{-Na_S d_S}\right)}{\left(1 - e^{-a_H d_H} e^{-a_S d_S}\right)}. \tag{S6}$$

From Equation (S6) we can define the effective area fraction of H_2O, Eqn. (S7), which we denote as the radiative area fraction, α_H^R, in the paper. The dependence of the radiative area fraction of H_2O on the absorption coefficient of SiO_2 can be understood by looking at the end-member cases. If the SiO_2 has a very low absorption, the radiative area fraction of the ice will be approximately 1 as radiation from the H_2O directly behind the SiO_2 grains will also emit radiation from the shock front. If the SiO_2 has an extremely high absorption coefficient, then the radiative area fraction will equal the physical area fraction, $\alpha_{H_2O}^P$, as the SiO_2 particles will absorb all the radiation from the H_2O directly behind.

$$\alpha_H^R = \left(\alpha_H^P + \alpha_S^P e^{-a_S d_S}\right) \tag{S7}$$

We can also define the effective emissivity for H_2O, ϵ_H^*, seen in Equation (S8). Here we have used the substituted the total thickness of the radiating H_2O and SiO_2 components, D_H and D_S, for $N \times d_H$ and $N \times d_S$, respectively.

$$\epsilon_H^* = \left(1 - e^{-a_H D_H} e^{-a_S D_S}\right) \frac{\epsilon_H}{\left(1 - e^{-a_H d_H} e^{-a_S d_S}\right)} \tag{S8}$$

Text S2: Experimental Details

As shown in Figure 2 of the main text, an off-axis Al-coated parabolic mirror collects and collimates radiance emitted from the downrange face of the sample through a CaF_2 window in the sample vacuum chamber. The mirror also focuses the incident and collects the reflected laser light for the velocity inteferometer (VISAR). The window through the target tank is Al_2O_3 protected by CaF_2. The collimated light is split with two dichroic beamsplitters between the Los Alamos near-infrared (NIR) pyrometer, the Ktech Model VMBV-04 velocity interferometer, and the Thorlabs Model PDA10A amplified Si diode visible detectors. The infrared pyrometer is sensitive to radiance temperatures as low as 300 K with a time resolution of 17 ns. The silicon diodes have a time resolution of 3 ns, and the visible filters were centered at 650 and 810 nm with full width half maximum of 100 and 30 nm, respectively. Emitted light is spatially filtered with a 17 mm diameter aperture so as to only collect light from the shocked sample. The optical path is enclosed in light-tight tubing to shield from the impact flash and propellant gases during the experiment. The system is calibrated with a Mikron M360 black body source (for the NIR) and an Optronic Laboratories OL-550 tungsten ribbon lamp (for the Si diode detectors), which are observed with the same optics and fibers as used in the experiments. The typical error in radiance is 2% at each wavelength. The NIR pyrometer data are recorded on 12-bit digitizers (e.g., Acqiris DC 440). The driver plate is lapped plane parallel and polished to an optical ($\sim$ 100 nm) finish to minimize thermal emission upon shock (Seifter et al., 2006). In two experiments (7.9 and 22.7 GPa), the ice-quartz mixtures were cold pressed directly onto the driver plate to reduce the gap between the driver and sample. The sample is affixed mechanically to the driver plate, which is cooled to $\sim$ 100 K by circulating liquid nitrogen. Initial temperatures of the samples were determined by a thermocouple on the driver plate. When the temperature of both the sample and driver are measured, the temperature deviation is typically less than 5 K. The sample vacuum chamber CaF_2 window is heated to prevent frosting. The velocity per fringe of the VISAR was 1896 m s^{-1}; two dropped fringes were added to the 22.7 GPa experiment presented in Figure 7. The VISAR spot size was large enough to average over $\sim$ 8 grains.

In the 18.5 GPa experiment, the SiO_2 was compacted and saturated with water, and then frozen in a manner similar to the preparation of polycrystalline columnar ice, as in Stewart et al. (2008). This preparation method produced a 40:60 H_2O to SiO_2 volumetric ratio with higher porosity than the evacuated cold press technique described in the main text. In this case, emission from trapped air prevented derivation of the shock temperature.

References

Carslaw, H. S., Jaeger, J. C., 1946. Conduction of Heat in Solids. Oxford University Press, USA, New York, NY.

Seifter, A., Stewart, S. T., Furlanetto, M. R., Kennedy, G. B., Payton, J. R., Obst, A. W., 2006. Post-shock temperature measurements of aluminum. In: Furnish, M. D., Elert, M., Russell, T. P., White, C. T. (Eds.), Shock Compression of Condensed Matter – 2005. American Institute of Physics, pp. 139–142.

Senft, L., Stewart, S., 2008. Impact crater formation in icy layered terrains on Mars. Meteorit. Planet. Sci. 43 (12), 1993–2013.

Steinberg, D., 1991. Equation of state and strength properties of selected materials. Tech. Rep. UCRL-MA-106439, Lawrence Livermore National Laboratory.

Stewart, S., Seifter, A., Obst, A., 2008. Shocked H_2O ice: Thermal emission measurments and the criteria for phase changes during impact events. Geophys. Res. Lett. 35, L23203, doi:10.1029/2008GL035947.

Wackerle, J., 1962. Shock-wave compression of quartz. J. Appl. Phys. 33, 922.